

# Frustration driven lattice distortion; an NMR investigation of $\text{Y}_2\text{Mo}_2\text{O}_7$

Amit Keren<sup>1</sup> and Jason S. Gardner<sup>2</sup>

<sup>1</sup>*Department of Physics, Technion - Israel Institute of Technology,  
Haifa 32000, Israel.*

<sup>2</sup>*NRC Canada, NPMR, Chalk River, Laboratories,  
Chalk River, Ontario, K0J 1J0 Canada.*

(Received: )

We have investigated the  $^{89}\text{Y}$  NMR spectrum and spin lattice relaxation,  $T_1$ , in the magnetically frustrated pyrochlore  $\text{Y}_2\text{Mo}_2\text{O}_7$ . We find that upon cooling the spectrum shifts, and broadens asymmetrically. A detailed examination of the low  $T$  spectrum reveals that it is constructed from multiple peaks, each shifted by a different amount. We argue that this spectrum is due to discrete lattice distortions, and speculate that these distortions relieve the frustration and reduce the system's energy.

PACS numbers:

*Geometric frustration* [1,2] occurs in magnetic systems where competition between magnetic nearest neighbor interactions and the local symmetry occurs. Geometrically frustrated magnets, such as those on a kagomé (2D) or pyrochlore (3D) lattice, often show signs of spin-glass-like behavior. Examples are the oxide pyrochlore compounds including  $\text{Y}_2\text{Mo}_2\text{O}_7$  [YMoO] [4–6],  $\text{Tb}_2\text{Mo}_2\text{O}_7$  [4,7],  $\text{Y}_2\text{Mn}_2\text{O}_7$  [8] and the kagomé based systems  $\text{SrCr}_8\text{Ga}_4\text{O}_{19}$  [9,10] and  $\text{Ba}_2\text{Sn}_2\text{Ga}_3\text{ZnCr}_7\text{O}_{22}$  [11]. Out of these, perhaps the best studied example is YMoO where detailed analysis of susceptibility measurements show both scaling and irreversibility [5] exactly as expected in conventional, chemically-disordered, spin glasses [12]. This is very intriguing since it is well established that glassiness requires BOTH randomness (disorder) and frustration [3]. In the kagomé case it was recently shown that the disordered magnetic sublattice is responsible for the glassiness [9]. However, the pyrochlore compounds are nominally disorder free. Therefore, the origin of their glassy behavior is still an open question.

Here we address this question by studying the internal magnetic field distribution in YMoO using  $^{89}\text{Y}$  NMR. Our major finding is a non-random distortion of the Mo sub-lattice starting at temperatures as high as 200 K. Such a distortion was previously detected by the EXAFS measurements of Booth *et al.* [13] at  $T = 15$  K. These distortions produce many non-equivalent  $^{89}\text{Y}$  sites and result in well separated, regularly spaced  $^{89}\text{Y}$  NMR peaks. We argue that such distortions can relieve the frustration and lower the systems energy, consequently resulting in various values of the spin-spin coupling constant,  $J$ , and the observed spin-glass-like behavior.

In YMoO, the magnetic Mo-ions and the non-magnetic Y-ions form two sub-lattices of corner-sharing tetrahedra. The sub-lattices interpenetrate in a way in which the Y is in the center of a Mo hexagon; pairs of Mo ions on this hexagon form the edges of the corner sharing tetrahedra.

The Y environment is shown in the inset of Fig. 1. Susceptibility measurements show that the spin-1,  $\text{Mo}^{4+}$  ions have an effective moment of  $2.55\mu_B$ . These moments interact antiferromagnetically, giving rise to a Curie-Weiss temperature  $\theta_{\text{cw}} = 200$  K [14]. The transition to the glassy state occurs at  $T_g = 22.5$  K, as measured by the irreversibility in field-cooled and zero-field-cooled magnetisation and is characterized by a strong suppression of spin fluctuations below this temperature [4,6]. The preparation of YMoO is described elsewhere [6]. Rietveld refinement of neutron powder diffraction data displays no sign of site exchange between Y and Mo or deviation from the nominal oxygen stoichiometry (an upper limit of 4% and 1% was placed respectively).

We obtain the NMR spectrum by sweeping the external field  $H_{\text{ext}}$  in a constant applied RF frequency  $f_{\text{app}} = 18.13$  MHz with a 50 G step size. For each field we apply a  $\pi/2$ - $\pi$  pulse sequence and record the entire time-dependent echo. We Fourier transform the recorded echo and shift the frequency scale by  $\Delta f = (^{89}\gamma/2\pi)(H_0 - H_{\text{ext}})$ ;  $H_0$  is the resonance field at  $T = 300$  K. We then add all the Fourier transforms to obtain the distribution of frequency differences  $\rho(\Delta f)$ . This method, known as the Fourier Step Sum (FSS) [15], allows one to construct the lines structures with the frequency resolution of the Fourier transform (5 kHz in our case) rather than on the larger FWHM spectrometer bandwidth (60 kHz in our case).

The sweeps at low temperatures were done in  $\sim 80$  different fields over 4kG. These sweeps took several days during which the temperature was kept constant to within 0.2 K. For a high  $T$  sweep we used 40 different field values. The integrated intensity (normalized by  $T$  due to the nuclear polarization) is similar in all temperatures indicating that we are detecting all the nuclear spins in the system. We also measured the spin lattice relaxation time,  $T_1$ , at different positions in the spectrum

to verify that our repetition rate is much longer than the longest  $T_1$ . At present our experiment is limited to liquid nitrogen temperatures due to the large spectral width at low  $T$  (to be demonstrated below) which results in low intensities at each applied field, and the difficulty of using high RF power below this temperature.

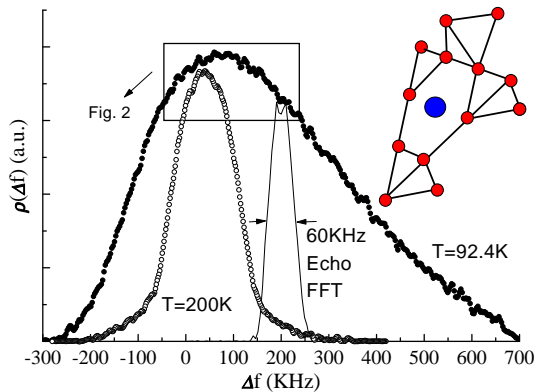


FIG. 1. The spectrum of the  $^{89}\text{Y}$  line at two temperatures. The units of the abscissa are arbitrary (for each  $T$ ) and are chosen for presentation purposes only. The marked area is replotted in Fig. 2. The inset shows the local environment of the  $^{89}\text{Y}$  in  $\text{Y}_2\text{Mo}_2\text{O}_7$ .

In Fig. 1 we plot  $\rho(\Delta f)$  at  $T = 200$  and  $92.4$  K using different arbitrary units for each line for presentation purposes. The high  $T$  spectra is nearly a perfect Gaussian except that some structure is seen at its top. In contrast, the low  $T$  spectra is not symmetric and the spectral weight shifts to high frequencies. In addition, the spectrum does not appear smooth but rather a combination of many peaks. In Fig. 1 we also present, with the use of a solid line, the FFT of a single echo obtained at  $H_{\text{ext}} = 8.515$  T but with the frequency shifted by  $(\gamma/2\pi)(H_0 - H_{\text{ext}})$ . This FFT shows a clear splitting at its top. This splitting is much larger than the noise of the FFT which is not observable on the scale of this figure. This FFT also demonstrates that the FWHM is 60 kHz.

In Fig. 2 we replot the area marked with a rectangle in Fig. 1 to reveal the rich structure in the spectrum. Clearly, it is a superposition of many distinct lines, each shifted by a different amount. The noticeable width of each peak is  $\sim 20$  kHz. It is therefore not surprising that these peaks, although noticeable in a standard field sweep experiment, are much better resolved using the FSS method. The FFT of the same single echo shown in Fig. 1 is depicted by the solid line in the right lower corner of Fig. 2; the splitting is much clearer here. Nevertheless, it is important to verify that the presence of a discrete set of lines is not due to the discrete number of external fields  $H_{\text{ext}}$ . Therefore, we present  $(^{89}\gamma/2\pi)(H_0 - H_{\text{ext}})$ , for all the  $H_{\text{ext}}$  we have applied, with open circles on the

abscissa. The 16 different NMR lines in the figure are obtained using 26 different external fields. Clearly, the peaks are incommensurate with the applied fields and are not a result of the spectrum construction method.

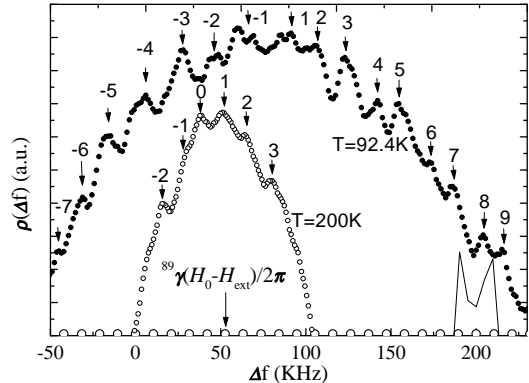


FIG. 2. The same as in Fig. 1 but only the center of the line is shown. Multiple peaks are observed in the spectrum and are indexed. In the  $T = 92.4$  K spectrum the index “0” is missing.

In Fig. 2 we index the frequencies  $\Delta f_{\text{max}}$  at which the peaks are found in an attempt to understand the spectrum. Only a portion of the indexes are shown. We found that at  $T = 200$  K,  $\Delta f_{\text{max}}(n)$  is a linear function of  $n$  as demonstrated in Fig. 3. A similar result is obtained at  $T = 92.4$  K (here the “0”th peak is missing). It is also important to mention that at temperatures higher than 200K, which is  $\theta_{\text{cw}}$ , we observed a smooth NMR line. Thus, below  $\theta_{\text{cw}}$  the NMR line is constructed from a set of resonance frequencies, and these frequencies are quantized.

Booth *et al.* argued that in YMoO the distortion is along the Mo-Mo bond, and not along the Y-Mo bond [13]. In addition, the absolute value of the NMR line shift indicates a field of  $\sim 1$  kG at the  $^{89}\text{Y}$  site, which cannot originate from dipolar coupling. Therefore, it is reasonable to assume that the dominant coupling between  $^{89}\text{Y}$  and the Mo-spin is transferred hyperfine and that it is uniform throughout the sample. This, combined with the observation of multiple peaks, leads us to the conclusion that in YMoO there is a discrete set of different local environments, each with its own local spin susceptibility  $\chi_{\text{loc}}$ . The relationship between this susceptibility and the observed frequency difference  $\Delta f$  is given by

$$\chi_{\text{loc}} \propto \frac{\Delta f}{f} \approx \frac{\Delta f}{f_{\text{app}}}. \quad (1)$$

The presence of a quantized set of NMR frequencies comes about because  $\chi_{\text{loc}}$  has discrete values.

Further information regarding the susceptibility distribution in YMoO was obtained by comparing the magne-

tization with the mean and width of the spectrum. We performed magnetization measurements in fields nearing the ones used for the NMR measurements. We found that  $M$  is a linear function of  $H$  at all the relevant temperatures. Therefore, we plot the inverse *macroscopic* susceptibility  $\chi_m^{-1} = H/M$  vs temperature in the inset of Fig. 4. The mean  $\langle \Delta f \rangle$  of  $\rho(\Delta f)$  is plotted vs.  $\chi_m$ , with the temperature as an implicit parameter, in Fig. 4. The error bars are taken as 10% of the FWHM. A linear relation is found. In addition, we characterize the NMR spectrum by the FWHM of  $\rho(\Delta f)$ , which is also depicted in Fig. 4 as a function of susceptibility. Again the dependence is linear, but the extrapolation of the FWHM to zero yields  $\chi_m = 0.035$  emu/gr. If the origin of the line width is frozen disorder (such as Y-Mo site exchange) we would expect  $\text{FWHM} \propto \chi_m$  (the susceptibility would be the only temperature dependent parameter). Since this is not the case, we conclude that the disorder must set in at the temperature where the  $\text{FWHM} > 0$ . From the extrapolation of the susceptibility data this should occur at  $T \sim 430$  K.

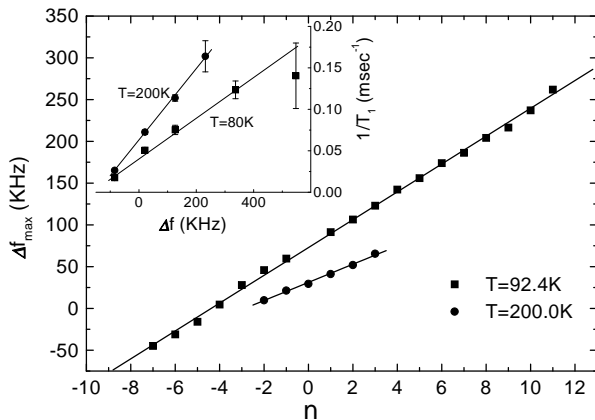


FIG. 3. The frequency differences at which the spectrum peaks  $\Delta f_{\max}$  is plotted vs. the index of the peak (see Fig. 2) for two different temperatures. A linear fit is shown by the solid lines. The inset shows the spin lattice relaxation rate,  $1/T_1$ , at different frequencies in the spectrum and at two different temperatures.

Dynamical information regarding the local environment could be obtained by measurements of the spin lattice relaxation rate  $1/T_1$  at different frequencies along the spectrum. The  $\Delta f$  dependence of  $1/T_1$  is plotted as an inset to Fig. 3, at two different temperatures. A linear dependence of the form  $1/T_1 = n + m\Delta f$  is found with  $n_{200} = 0.062(1)$  and  $n_{80} = 0.040(1)$   $\text{msec}^{-1}$ , and  $m_{200} = 4.2(1) \times 10^{-4}$  and  $m_{80} = 2.6(2) \times 10^{-4}$ , where the subscript is the temperature at which  $n$  and  $m$  were evaluated. Interestingly, the average  $\langle 1/T_1 \rangle = n + m \langle \Delta f \rangle$  is  $0.08 \text{ msec}^{-1}$  for both temperatures.

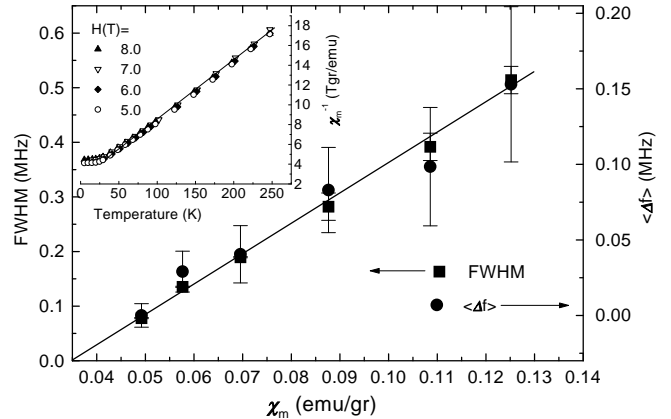


FIG. 4. The mean and FWHM of the frequency difference distribution  $\rho(\Delta f)$  versus susceptibility. The inset is the inverse macroscopic DC-susceptibility  $H/M$  vs. temperature at several fields between 5 and 8 T.

Now we would like to discuss the possible origin of the multiple distinct local environments. The simplest scenario is that they emerge from impurities, which, in principal could generate alternating magnetic fields in their vicinity. However, the amount of disorder in the sample, the fact that it must be temperature dependent, the theoretical expectation of fast healing (even in the ground state an impurity impacts only its nearest neighbor) [16], and the experimental observation of short correlation length ( $< 0.5$  nm) [6] all point away from this possibility. The other option is lattice distortions. It is conceivable that such a distortion relieves the frustration and reduces the total system energy; this was discussed theoretically in detail for classical spins [17], quantum spin [18], and by numerical simulations [19]. For simplicity we demonstrate the idea of frustration driven lattice distortion here on the 2-dimensional kagomé lattice of corner sharing triangles. In Fig. 5 we show a kagomé lattice where all the bonds are identical. In this case the energy,  $E$ , per number of bonds  $N$ , is  $E/N = -J$ . We also show a distorted kagomé lattice where there are three types of interactions with coupling constants  $J$ , as before,  $J_b$  (bigger than  $J$ ) for the shorter bonds, and  $J_s$  (smaller than  $J$ ) for the longer bonds. In this case the main objective of the spins is to satisfy the shorter bonds. One way of doing this is by rearranging themselves into a collinear spin configuration as demonstrated in the figure. In this case, and provided that  $J_s + J_b = 2J$ , we find  $E/N = -(2/3)J_b$  so that if  $J_b > (3/2)J$  the lattice has magnetic “motivation” to distort.

In the 3D pyrochlore lattice the situation is more complicated since theoretically a collinear spin configuration belongs to the ground state manifold. In addition, the reduction of magnetic energy competes with an increase of the elastic energy due to the distortion, and, at present, it is not clear that YMoO will benefit energetically from

such a distortion. Even less clear is the reason why the distortion should lead to the discreteness of sites. However, the recent finding that the two-dimensional  $S = 1/2$  frustrated antiferromagnet  $\text{Li}_2\text{VOSiO}_4$  system also distorts prior to its spin freezing [20] is encouraging.

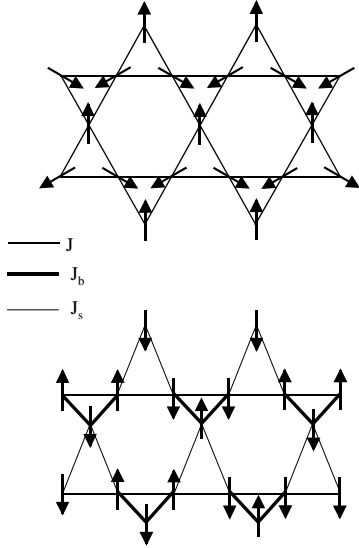


FIG. 5. Schematic demonstrating the concept of frustration induced distortion for the kagomé lattice. (a) Before the distortions the coupling between all spins is  $J$ . (b) When odd lines move up, the coupling between spin on diagonal lines is either bigger ( $J_b$ ) or smaller ( $J_s$ ) than  $J$  depending on the length of the bond. If  $J_b > 1.5J$  the spin arrangement in panel (b) has a lower magnetic energy than the one in panel (a). The system might therefore prefer to distort.

In conclusion we have evidence from  $^{89}\text{Y}$  NMR of multiple discrete values of the local susceptibility at the Y sites in the spin glass like pyrochlore  $\text{Y}_2\text{Mo}_2\text{O}_7$ . We speculate that this is a result of small discrete changes in the Mo-Mo bond lengths which are detectable in NMR at  $T < 200$  K. We suggest that this distortion relieves the geometric frustration allowing the system to enter a unique ground state. We believe these new experimental observations beg for more theoretical and experimental investigation of frustration driven lattice distortions.

The authors would like to thank P. Mendels and M. Horvatić for helpful discussion. A. Keren would like to thank the Israel - U. S. Binational Science Foundation for supporting this research.

- [2] For recent reviews see: A.P. Ramirez, *Annu. Rev. Mater. Sci.*, **24**, 453, (1994); *Magnetic Systems with Competing Interactions*, edited by H.T. Diep (World Scientific, Singapore, 1994); P. Schiffer and A.P. Ramirez, *Comm. Cond. Mat. Phys.*, **18**, 21, (1996).
- [3] K. Binder and A. P. Young, *Rev. Mod. Phys.* **58**, 801 (1986).
- [4] S.R. Dunsiger, R. F. Kiefl, K. H. Chow, B. D Gaulin, M. J. P. Gingras, J. E. Greedan, A. Keren, K. Kojima, G. M. Luke, W. A. MacFarlane, N. P. Raju, J. E. Sonier, Y. J. Uemura, and W. D. Wu, *Phys. Rev. B* **54**, 9019 (1996).
- [5] M.J.P. Gingras, C.V. Stager, N.P. Raju, B.D. Gaulin and J.E. Greedan, *Phys. Rev. Lett.* **78**, 947 (1997).
- [6] J.S. Gardner, B.D. Gaulin, S.-H. Lee, C. Broholm, N.P. Raju, and J.E. Greedan, *Phys. Rev. Lett.* **83**, 211 (1999).
- [7] B. D. Gaulin, J. N. Reimers, T. E. Mason, J. E. Greedan, and Z. Tun, *Phys. Rev. Lett.* **69**, 3244 (1992).
- [8] J.N. Reimers, J. E. Greedan, R. K. Kremer, E. Gmelin, and M. A. Subramanian, *Phys. Rev. B* **43**, 3387 (1991).
- [9] P. Mendels, A. Keren, L. Limot, M. Mekata, G. Colin, and M. Horvatić, *Phys. Rev. Lett.* **85**, 3496 (2000).
- [10] X. Obradors *et al.*, *Solid State Commun.* **65**, 189 (1988); A. P. Ramirez, G.P. Espinosa and A.S. Cooper, *Phys. Rev. Lett.* **64**, 2070 (1990).
- [11] I. S. Hagemann, Q. Huang, X. P. A. Gao, A. P. Ramirez, and R. J. Cava, *Phys. Rev. Lett.* **86**, 894 (2001).
- [12] J. A. Mydosh, **Spin Glasses** (Taylor and Francis, London) 1993.
- [13] C. H. Booth, J. S. Gardner, G. H. Kwei, R. H. Heffner, F. Bridges and M. A. Subramanian, *Phys. Rev. B.* **62**, R755 (2000).
- [14] N. P. Raju, E. Gmelin and R. K. Kremer, *Phys. Rev. B* **46**, 5405 (1992).
- [15] W. G. Clark, M. E. Hanson, and F. Lefloch, *Rev. Sci. Instrum* **66**, 2453 (1995).
- [16] J. Villain, *Z. Physik B* **33**, 31 (1979).
- [17] K. Terao, *JPSJ* **65**, 1413 (1996).
- [18] Y. Yamashita and K. Ueda, *Phys. Rev. Lett.* **85**, 4960 (2000).
- [19] L. Bellier-Castella, M. J. P. Gingras, P.C.W. Holdsworth and R. Moessner, cond-mat 0006306.
- [20] R. Melzi, S. Aldrovandi, F. Tedoldi, P. Carretta, P. Millet, F. Mila, *Phys. Rev. Lett.* **85**, 1318 (2000).

[1] G. Toulouse, *Commun. Phys.* **2**, 115 (1977).